REPORT DOCUMENTATION PAGE

Form Approved
OMB No. 0704-0188

1. AGENCY USE ONLY (*Leave Blank*)	2. REPORT DATE	3. REPORT TYPE AND DATES COVERED
	96APR23	95MAY09 - 96JAN 16 FINAL

4. TITLE AND SUBTITLE
HIGH EFFICIENCY AlInGaP VISIBLE VERTICAL CAVITY LASERS INCORPORATING WAFER FUSION AND IMPROVED HEAT SINKING

5. FUNDING NUMBERS

6. AUTHOR(S)
VIJAYSEKHAR JAYARAMAN

7. PERFORMING ORGANIZATION NAME(S) AND ADDRESS(ES)
OPTICAL CONCEPT, INC.
P.O. BOX 668
LOMPOC, CA 93436

8. PERFORMING ORGANIZATION REPORT NUMBER
F0053

9. SPONSORING/MONITORING AGENCY NAME(S) AND ADDRESS(ES)
US ARMY SPACE AND STRATEGIC DEFENSE COMMAND
P,O. BOX 1500
HUNTSVILLE, AL 35807-3801

10. SPONSORING/MONITORING AGENCY REPORT NUMBER

11. SUPPLEMENTARY NOTES

12a. DISTRIBUTION/AVAILABILITY STATEMENT
UNLIMITED DISTRIBUTION

12b. DISTRIBUTION CODE
UL

13. ABSTRACT (*Maximum 200 words*)

Red vertical cavity surface emitting lasers (VCSELs) using aluminum indium gallium phosphide (AlInGaP) based active regions are limited in performance by thermally aqctivated carrier leakage, and absorption in alluminum gallium arsenide mirrors. This program seeks to improve performance by flip-chip bonding for better heat sinking. This requires wafer fusion to gallium phosphide substrates We also improve device efficiency by lateral oxidation. Lastly, we investigate alternative mirror combinations which are transparent to shorter wavelengths.

14. SUBJECT TERMS
visible laser - vertical cavity - wafer fusion - flip-chip bonding - GaInP - lateral oxidation

15. NUMBER OF PAGES
27

16. PRICE CODE

17. SECURITY CLASSIFICATION OF REPORT	18. SECURITY CLASSIFICATION OF THIS PAGE	19. SECURITY CLASSIFICATION OF ABSTRACT	20. LIMITATION OF ABSTRACT
Unclassified	Unclassified	Unclassified	SAR

DISCLAIMER NOTICE

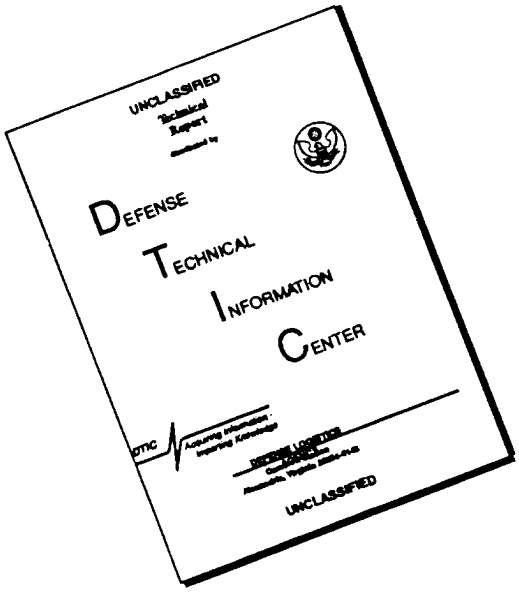

THIS DOCUMENT IS BEST QUALITY AVAILABLE. THE COPY FURNISHED TO DTIC CONTAINED A SIGNIFICANT NUMBER OF PAGES WHICH DO NOT REPRODUCE LEGIBLY.

High-Efficiency AlInGaP Visible Vertical Cavity Surface-Emitting Lasers Incorporating Wafer Fusion and Improved Heat Sinking

BMDO Contract DASG60-95-C-0053

Phase I Final Report

Optical Concepts
432A Commerce Ave.
Lompoc, CA 93436

High-Efficiency AlInGaP Visible Vertical Cavity Surface-Emitting Lasers Incorporating Wafer Fusion and Improved Heat-Sinking

Phase I Final Report

I. Introduction and Review of Phase I Objectives

As described in our phase I proposal, this work set out to improve the perfromance of visible vertical cavity surface-emitting lasers (VCSELs) using Aluminum Indium Gallium Phosphide (AlInGaP)-based active regions grown on Gallium Arsenide (GaAs) substrates. At the time this work began, the shortest operating wavelength of red VCSELs was 670 nm [1], using the structure of Fig. 1.1. The goals of this program were extending the operating wavelength down to at least the plastic fiber wavelength of 650 nm, and improving temperature range of operation. These two goals are very much related, and limited by the same fundamental problem. In the AlInGaP material system used for red light generation, the confinement of electrons in InGaP quantum wells surrounded by AlInGaP barriers is weak. Shortening wavelength or increasing temperature causes electrons to leak out of the quantum wells, which inhibits lasing efficiency.

There are essentially two approaches to solving this problem. The first approach is simply to increase device efficiency by decreasing intracavity optical loss, which reduces the drive power required for a given output power. This in turn reduces the amount of heat input to the device. The second approach is to improve the conduction of heat away from the cavity, so that a given amount of heat input to the cavity results in a smaller temperature rise. Figure 1.2 shows a device structure that incorporates both of these approaches. The device is "wafer-fused" to a transparent Gallium Phosphide (GaP) substrate so the device can emit through the substrate. Conventional red VCSELs, as shown in Fig. 1.1, are forced to be top-emitting, because the GaAs substrate is absorbing. Using a bottom-emission structure allows the device to be "flip-chip bonded," which enhances heat conduction away from the device. Also shown in Fig. 1.2 is current and optical confinement through lateral oxidation of an AlGaAs layer, as has been demonstrated in 980 nm VCSELs [2]. This reduces optical loss, and indirectly reduces heat by reducing the amount of required drive power. The structure of Figure 1.2 could be further improved by using an AlInP/Al_XO_Y or AlGaAs/Al_XO_Y mirror structure instead of AlGaAs/AlAs mirrors. The Al_XO_Y based mirror structures are transparent to shorter wavelengths than the

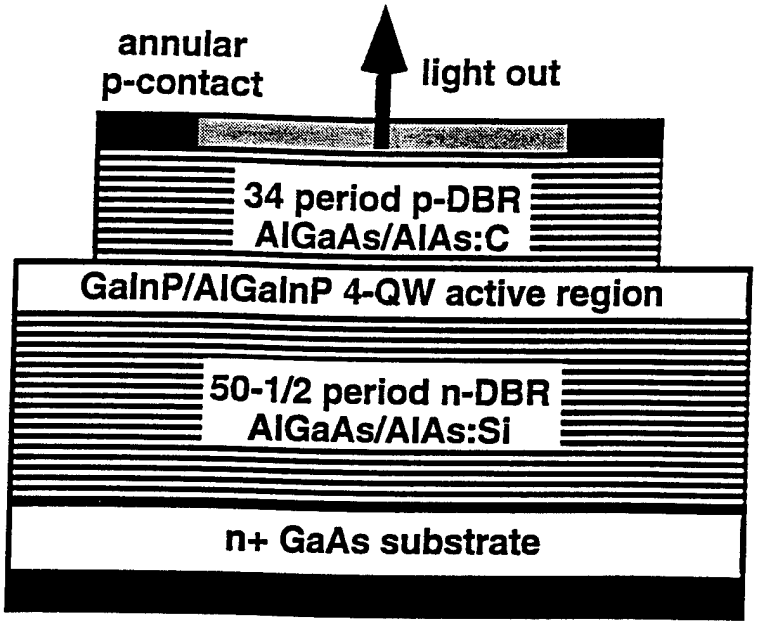

Figure 1.1: Schematic of top-emission red VCSEL.

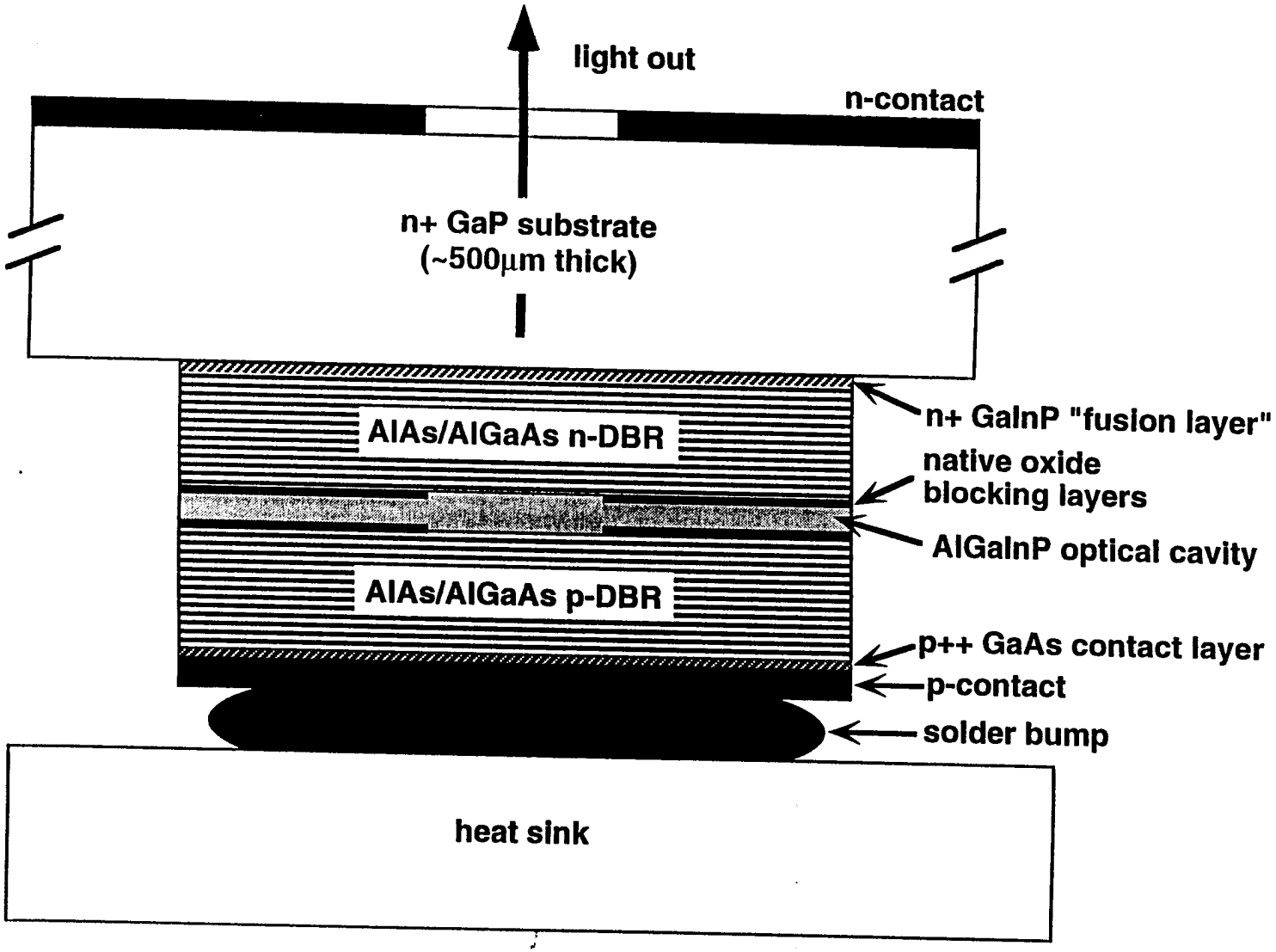

Figure 1.2: Bottom-emission wafer-fused red VCSEL with lateral oxidation and flip-chip bonding.

conventional AlAs/AlGaAs mirrors. This allows shorter wavelength operation with lower loss mirrors.

Our goal in phase I was to demonstrate the feasibility of a structure like that of Fig. 1.2. Our goal was broken down into the following intermediate objectives in our phase I proposal :

1. Demonstrate wafer fusion of GaP to GaAs.

2. Demonstrate Al_XO_y current-blocking layers in conventional (absorbing substrate) AlInGaP-based red VCSELs.

3. Demonstrate high-reflectivity AlInP/Al_XO_y distributed Bragg reflectors.

4. Demonstrate transparent-substrate VCSELs using wafer-fusion to GaP substrates and selective oxidation for current injection.

5. Fabricate transparent-substrate visible VCSELs using wafer fusion (objective 1), selectively oxidized current blocking layers (objective 2), and AlInP/Al_XO_y distributed Bragg reflectors (objective 3).

Objectives 1-5 represent an extremely ambitious set of goals for phase I. Needless to say, not all the objectives were fully met. Objectives 1-3 represent technology "pieces," while objectives 4 and 5 attempt to combine these pieces into complex high-performance devices. In this phase I program, objectives 1-3 were essentially completed, objective 4 was partially completed, and objective 5 was not completed. It was determined, however, that AlInP mirrors are not necessary to obtain continuous-wave (CW) VCSELs in the 650 nm range, although they may ultimately improve performance. We show CW 645 nm VCSELs in Section III using conventional AlAs/$Al_XGa_{1-X}As$ mirrors. In Section IV, we show that $Al_XO_y/Al_XGa_{1-X}As$ mirrors are also suitable for high index contrast, low absorption mirrors at 630-650 nm, and these rely on a simpler and more established growth technology than the AlInP/Al_XO_y mirrors we originally proposed.

In pursuing objectives 1-4, several advances in visible VCSELs have been made during this program. In particular, the operating wavelength of red VCSELs has been reduced to the all-important 650 nm window for plastic fiber optical communication, primarily as a result of objective 2 above being met by our subcontractor Sandia National Laboratories. In addition, we have demonstrated conversion of an absorbing substrate

resonant cavity LED into a tranparent substrate resonant cavity LED using wafer fusion and substrate removal. Although our original intent was to accomplish this using a red VCSEL wafer, no such wafer was available during the course of this program. This has been due primarily to personnel changes at Sandia National Laboratories, combined with the challenges of growing red VCSEL epitaxy. We have therefore demonstrated a wafer-fused transparent substrate LED using a near-infrared VCSEL wafer operating at 780 nm and grown on GaAs. This VCSEL wafer did not lase, for reasons we discuss in Section IV, but exhibited good I-V characteristics, and emitted light through the substrate with low optical loss. Like red VCSELs, 780 nm VCSELs or resonant cavity LED's are normally forced to be top-emitting devices because the GaAs substrate is absorbing. By replacing the substrate with a transparent GaP substrate using wafer fusion, however, we have fabricated bottom-emission 780 nm devices, described in Section V. The bottom-emission geometry will allow future devices to use flip-chip bonding for improved heat-sinking. Our simple demonstration opens the door for the same geometry being employed with red VCSELs in the future.

The remainder of this report is organized as follows. In section II, we discuss our results in wafer-fusing GaP to GaAs. We then discuss the work of our subcontractor Sandia National Laboratories (SNL) in selectively oxidized red VCSELs, and in reducing the wavelength of red VCSELs to 645 nm. Section IV reviews work by OCI engineer Michael MacDougal at the University of Southern California, in developing Al_xO_y-based mirrors. Before concluding in Section VI, we discuss our resonant cavity 780 nm bottom-emission LED results in Section V.

II. Wafer Fusion of GaP to GaAs

A. Obtaining strong mechanical adhesion.

An important result of this phase I investigation is that we were able successfully to wafer-fuse GaP to GaAs. A rather surprising result of our investigation was that an Indium-containing layer at the fusion interface does not necessarily enhance fusion. Previous authors have suggested this Indium containing layer should improve things [3]. Figure 2.1 illustrates the two epilayer structures we employed in our initial investigation of wafer fusion. In one case, we included an InGaP "adhesion layer" during fusion, and in the other case we omitted it. Surprisingly, the InGaP layer did not lower the the temperature required for fusion, contrary to our

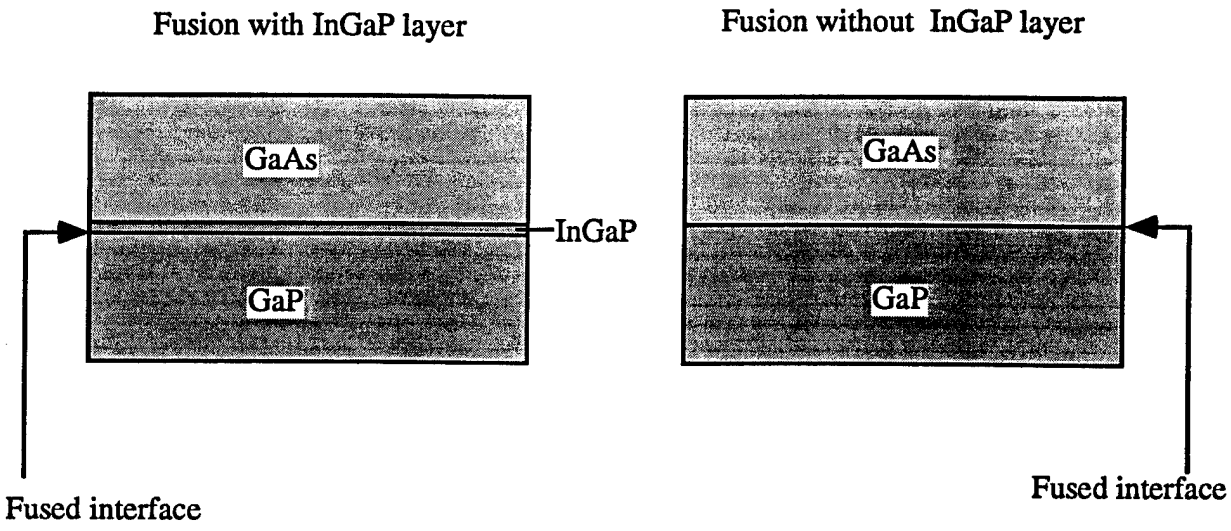

Table I

	670 °C; 0.5 hour	700 °C; 0.5 hour	750 °C; 0.5 hour
With InGaP layer	Did not fuse	Fused over 8 mm by 8 mm sample	Fused over 8 mm by 8 mm sample
Without InGaP layer	Fused over half of 8 mmX 8 mm sample	Fused over 8 mm by 8 mm sample	Fused over 8 mm by 8 mm sample

Figure 2.1: Fusion experiments with and without InGaP layer. The successful fusion without the InGaP layer was obtained with both misoriented (100) and (311) substrates.

expectations. Table I summarizes our results. As shown, we attempted wafer fusion at 670°C, 700 °C, and 750°C. With or without the InGaP layer, we obtained fusion at 700 °C and 750°C, using a fusion time of 1/2 hour. At 670°C, the sample without the InGaP layer showed fusion over a portion of the sample, while that with the InGaP layer did not fuse at all. This suggests that the InGaP layer actually raises the required fusion temperature, but more experiments are required to demonstrate this conclusively. At any rate, none of our experiments indicate that it is necessary, so we have eliminated it in future experiments. Also, using the 700 °C fusion temperature, we obtained successful fusion with substrates misoriented from (100) and with (311) substrates.

Figure 2.2 shows in more detail the temperature cycling employed in the wafer fusion process of GaP to GaAs, without the adhesion layer. Fig. 2.2 also shows some additional details of the cleaning procedure used prior to fusion. It is possible this procedure affects the minimum temperature for fusion, but in our experiments with various cleaning procedures, we were not able to reduce the fusing temperature below that shown in Table I. All of our subsequent fusion of GaP to GaAs has therefore used the procedure of Fig. 2.2.

A number of criteria can be used to evaluate the quality of the fused inteface. Fortunately with a transparent substrate like GaP, a cosmetic evaluation is particularly easy. Simply looking through the back (GaP side) reveals how much of the area has fused. Figure 2.3 shows optical microscope photos of good and bad wafer fusion of GaAs to GaP, viewed through the GaP substrate. The dark areas represent fused areas, and the light areas are places where there is still an air gap between the surfaces. Good wafer fusion is represented by a completely dark picture. In non-fused areas, it is often common to observe a fringe pattern. The air gap creates a resonant cavity with laterally varying thickness, creating lateral fringes. These fringes move laterally as pressure is applied to the sample and the air gap thickness is varied, providing another indication that fusion has not occurred in this area. Another good cosmetic evaluation is provided by scanning electron microscope (SEM) photos. Figure 2.4 shows an SEM of a 780 nm VCSEL (made of GaAs/AlGaAs) wafer-fused to a GaP substrate. We will discuss this VCSEL structure in more detail in Section V. The point here is that there are no visible voids at the fused interface.

B. Optical and Electrical Characteristics

We performed no quantitative measurements of the optical quality fused GaAs/GaP interfaces, because we feel confident that if no voids are visible at the fused interface, then

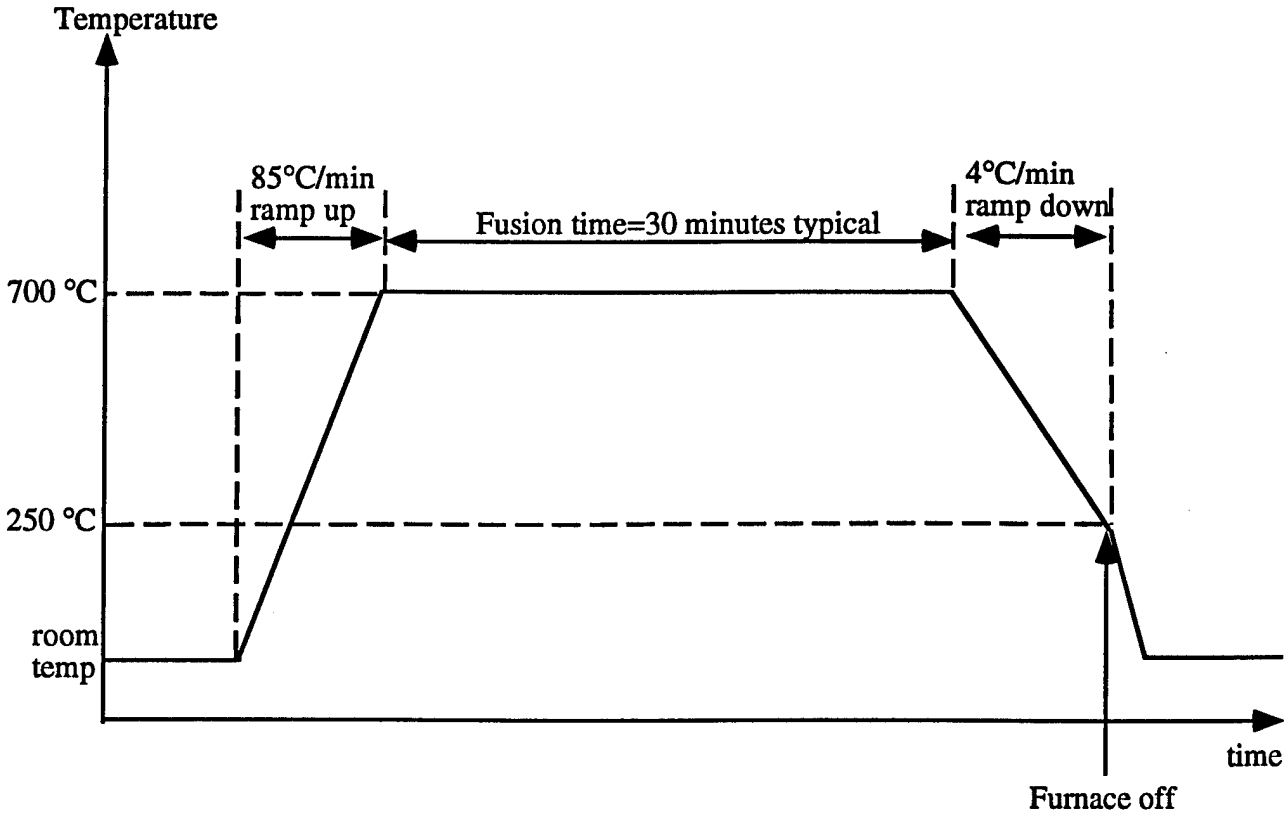

Cleaning procedure:

1. Ultrasonic cleaning with solvents.
2. Strip native oxide with Hydroflouric acid
3. Water rinse and dry.
4. Strip oxide again with ammonium hydroxide.
5. Methanol rinse
6. Load in fusion fixture and load into furnace.

Figure 2.2: Wafer fusion thermal cycling and cleaning procedure.

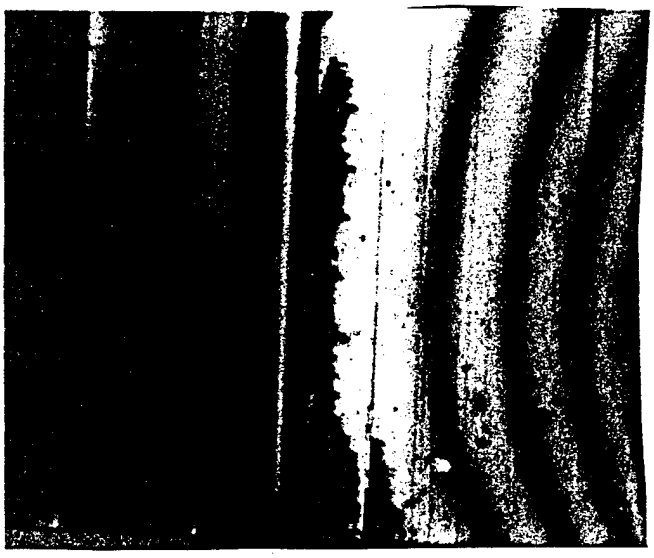

Figure 2.3: Optical micrscope photo through GaP side of GaP fused to GaAs. The fringes indicate unfused areas. The solid dark areas are where fusion has occurred.

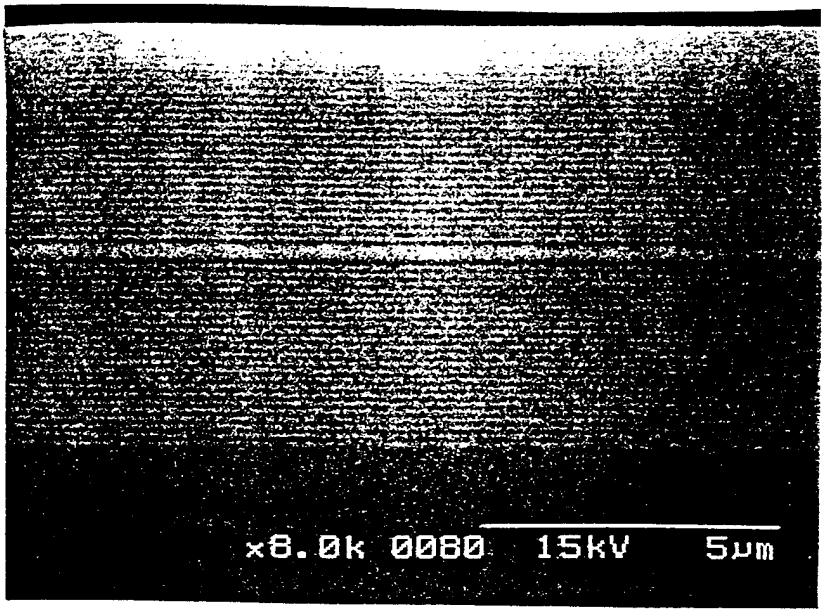

Figure 2.4: Scanning electron micrograph (SEM) of 780 nm VCSEL structure fused to a GaP substrate. The absence of voids indicates low optical scattering loss.

optical scattering loss is negligible. This is particularly true when the fused junction is external to the laser cavity, as it is in the device structures we discuss in this proposal. External to the laser cavity, if our scattering loss is for example 5 percent, the only effect on device performance is a 5 percent reduction in output power. Our experience with wafer fusion of GaAs to InP is that we routinely achieve much lower optical losses inside wafer-fused 1550 nm VCSEL cavities. Based on observed external efficiencies in 1550 nm VCSELs, we estimate <0.2 % per pass scattering loss in a fused GaAs/InP junction [4]. Similar numbers can be expected in GaAs/GaP wafer fusion.

Electrical characteristics of the fused junction are less important, because the n-contact in the device can be placed in the n-mirror instead of the backside of the substrate, as described in Fig. 5.2. This eliminates the need for pumping current across the fused junction. Nevertheless, in Section V, we compare I-V characteristics for contact placed in the n-mirror, and contact on the back of the substrate. Section V indicates a small additional voltage from fusion, but generally good conduction across the fused interface.

C. Temperature-cycled in-plane lasers

An important question in the fabrication of fused red VCSELs is does the InGaP active region degrade under the temperature cycling associated with wafer fusion? (See Section II.a for a description of temperature cycle.) Unfortunately, the experiment we performed along these line was inconclusive, although encouraging. Our experiment was the following. We took a piece of *in-plane* laser material, and processed in-plane lasers before and after thermally cycling a portion of the material. The temperature cycle we chose was 60 minutes at 700 °C, with ramp-up and ramp-down times like those in Fig. 2.2. This is longer than the 30 minute time we later concluded was adequate. Figure 2.5 shows the measured L-I curves of broad-area lasers from cycled and uncycled material, under pulsed operation. Both threshold and differential efficiency are slightly higher and lower, respectively, for the cycled sample, than for the uncycled sample. The uncycled sample exhibits a threshold current density of 0.946 kA/cm^2, while the cycled sample shows 1.18 kA/cm^2 broad-area threshold current density. The uncycled sample showed a differential efficiency of 0.51 Amps/watt,. while the cycled sample showed 0.35 Amps/watt. This suggests the radiative efficiency of the temperature-cycled InGaP/AlInGaP active material is slightly worse, although lasing was observed in both samples. Further statistical data is required to state this conclusively, since the amount of variation observed is within that commonly observed from device to device on a given wafer. Nevertheless, both samples lase at comparable thresholds and output powers, and if the degradation is real, it is

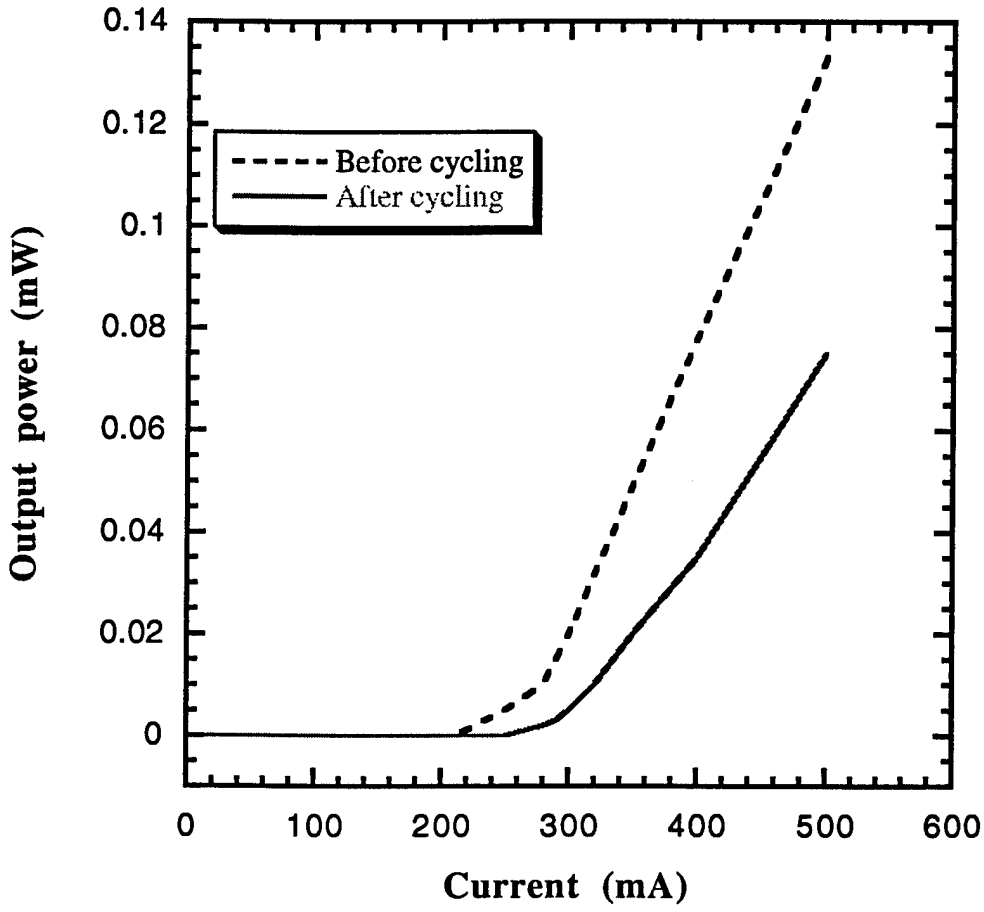

Figure 2.5: L-I curves before and after thermal cycling.

possible that simply reducing the fusion time from 1 hour to 0.5 hour (see Fig. 2.2) may solve the problem. We showed earlier that 30 minutes is adequate for wafer fusion.

If it is later demonstrated that active regions degrade unacceptably even after 30 minute fusion time at 700 °C, there a number of ways to significantly decrease the bonding temperature. One option arises from placing the n-contact in the n-mirror, as described above and in Section V. This eliminates the need for an electrically conductive bonding junction, and may eliminate the need for wafer fusion entirely. Figure 2.6 shows an approach without wafer fusion. Instead of a wafer-fused bond, it is possible to use a Palladium bond, using approximately 50 Å of Palladium Palladium bonds can be formed at as low as 200 °C, and bond strength at 400 °C is extremely good. At such low temperatures, we can assert confidently that optical quality will remain unchanged.

An aperture in the Palladium allows light to pass through, creating a bottom emission device as desired. Although the heat conduction through an air gap is potentially very poor, because the air gap is thin, and because of lateral heat-spreading above and below the air gap, the thermal impedance of the device will not be greatly compromised.

III. AlInGaP/AlGaAs-based Red VCSELs with Al_xO_y Current Blocking Layers-Sandia Results

The original work by Schneider, et al [1] on red VCSELs used an ion-implanted structure as shown in Fig. 1.1. In 980 nm lasers, the best results have been obtained using an oxide aperture structure [2], which introduces less scattering loss, and allows smaller devices to be fabricated with less leakage current than the ion-implanted structure. A logical path to follow in red VCSEL development, therefore, is to fabricate oxide-aperture devices to reduce threshold and therefore reduce heating. This in turn should allow reduction of the operating wavelength, as discussed in the introduction. Our subcontractor Sandia National Laboratories has followed this path successfully, as discussed in this section.

Sandia's work, spearheaded by Choquette, et al, has achieved continuous-wave (CW) operation at 642 nm and is summarized in [4]. Previous work was primarily in the 670-690 nm wavelength range. This is significant because the anticipated plastic fiber communication market requires operation at 650 nm. Figure 3.1 shows the basic structure of the device. These lasers are grown using low-pressure metal-organic vapor-phase epitaxy (MOVPE) on (311) GaAs substrates. The AlGaAs distributed Bragg reflectors (DBRs) make use of parabolic compositional grading in conjunction with Carbon and Silicon dopants, as previously demonstrated by Sandia in 980 nm VCSEL work. This

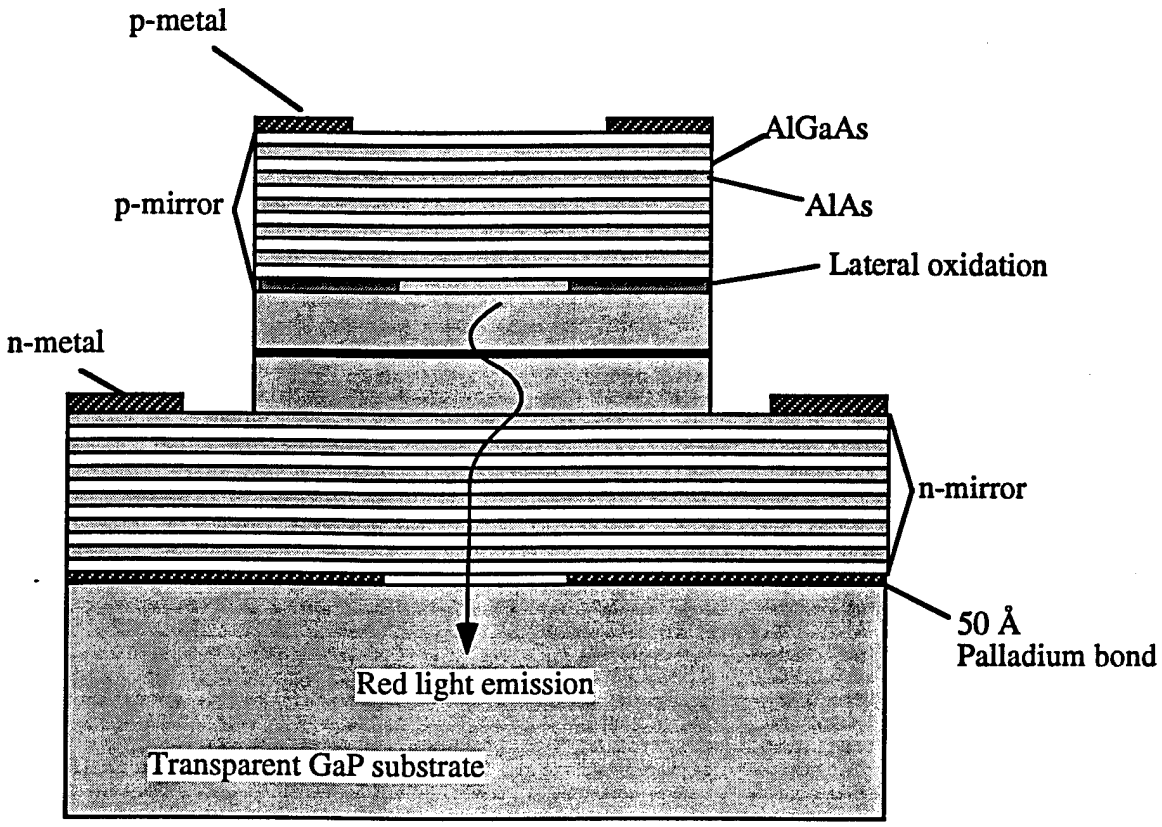

Figure 2.6: Realizing a bottom-emission device with low-temperature Palladium bonding instead of wafer fusion. The Palladium is thin, so that the aperture does not significantly compromise thermal impedance. Also, the n-contact is in the mirror, so there is no need for a conducting bonding junction.

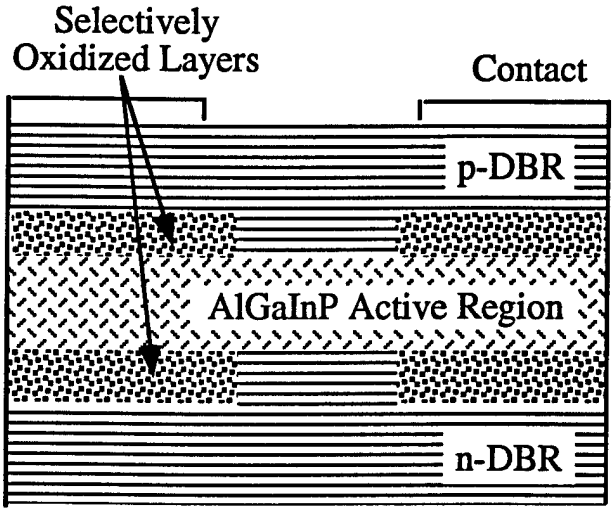

Figure 3.1: Red VCSEL structure with lateral oxidation.

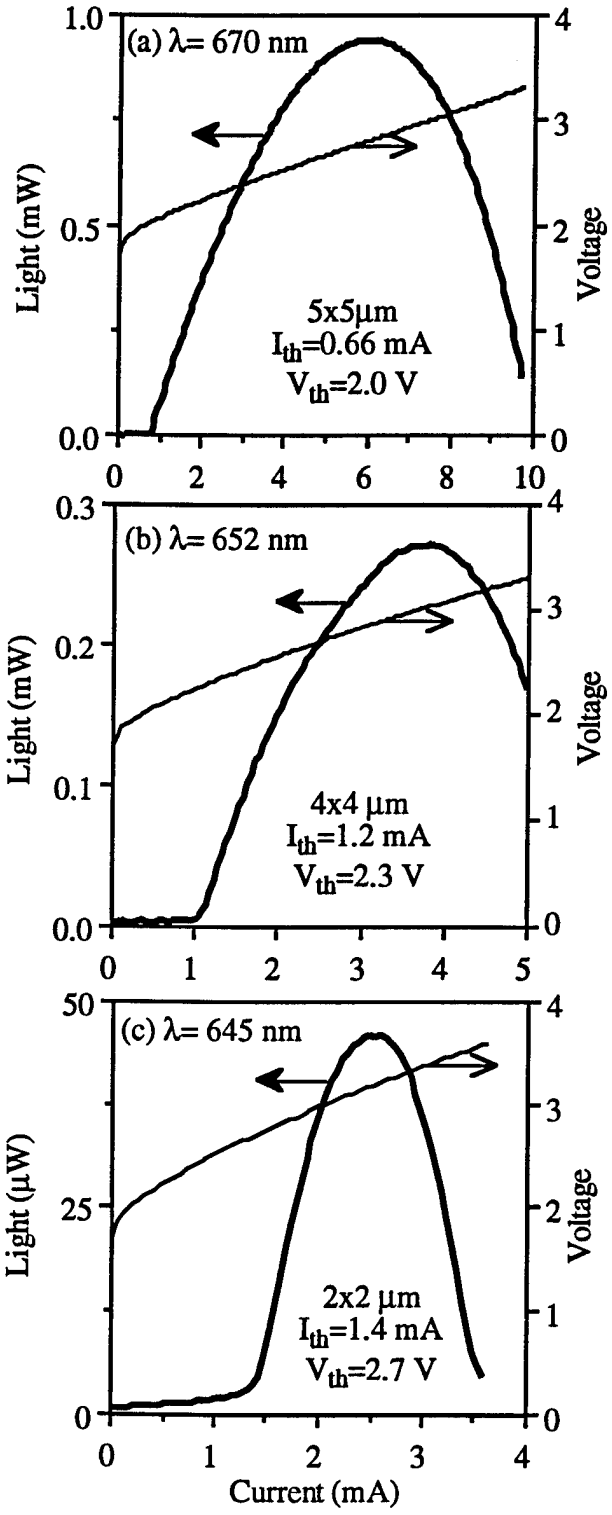

Figure 3.2: L-I Curves of various devices fabricated with lateral oxidation. The smallest two devices lased at wavelengths short enough for plastic fiber communication.

contributes to not only low threshold current but also low threshold voltage. The active region consists of 4 compressively strained InGaP quantum wells.

The confinement of current and optical energy is accomplished by lateral oxidation of 2 high aluminum content AlGaAs layers adjacent to the active region, one above it and one below it, as indicated in Fig. 3.1. The current apertures tested varied from 2 μm X 2 μm to as large as 19 μm X 19 μm. For the purposes of this program, the most interesting results are provided by the smaller sizes, since these lased at the shortest wavelengths. Figure 3.2 indicates the L-I curves of 3 different devices. The 4 X 4 μm^2 device lased at 652 nm with 280 μW maximum CW power, and the 2 X 2 μm^2 device lased at 645 nm, with nearly 50 μW of output power. This demonstrates conclusively that red VCSELs can operate at the 650 nm plastic fiber window. Although considerable development is required to increase output power and temperature range of operation, the initial results look very promising.

IV. Alternative mirror technologies

Although red VCSELs with conventional AlAs/AlGaAs mirrors can operate down to 645 nm as shown in Section III, shortening wavelength much below this is difficult, because the high index AlGaAs becomes absorbing. Even at 645 nm operation, the $Al_xGa_{1-x}As$ portion of the mirror is close to its band-edge, and is also absorbing. The natural design course is to increase the Aluminum content in the AlGaAs (increase x-value) to push its absorption edge to shorter and shorter wavelengths, but this reduces its refractive index. Fig. 4.1 illustrates the refractive index of $Al_xGa_{1-x}As$ for different x values, as a function of wavelength. For each x-value, the curve ends at the left edge at the band-edge. For a given x-value, the band-edge wavelength is given by [5]:

$$\lambda_{abs}=1.24 \ / \ (1.424+1.266x+0.26x^2)$$

For a low loss mirror, we would like the lasing wavelength ideally to be 50-100 nm longer than the absorption edge of both high and low index materials in the DBR. For the Helium Neon wavelength of 632 nm, for example, this forces us to use x-values greater than 0.7-0.8. The resulting AlAs/$Al_{.8}Ga_{.2}As$ DBR has a maximum refractive index contrast of 0.2-0.3, which is less than half that available for 980 nm VCSELs. With a small refractive index contrast, more mirror periods are required for sufficient reflectivity, putting greater stress on epitaxial growth, and increasing sensitivity to diffraction, scattering and absorption losses. As a result, for operation at the Helium-Neon wavelength of 632 nm, some other choice of mirrors is likely required.

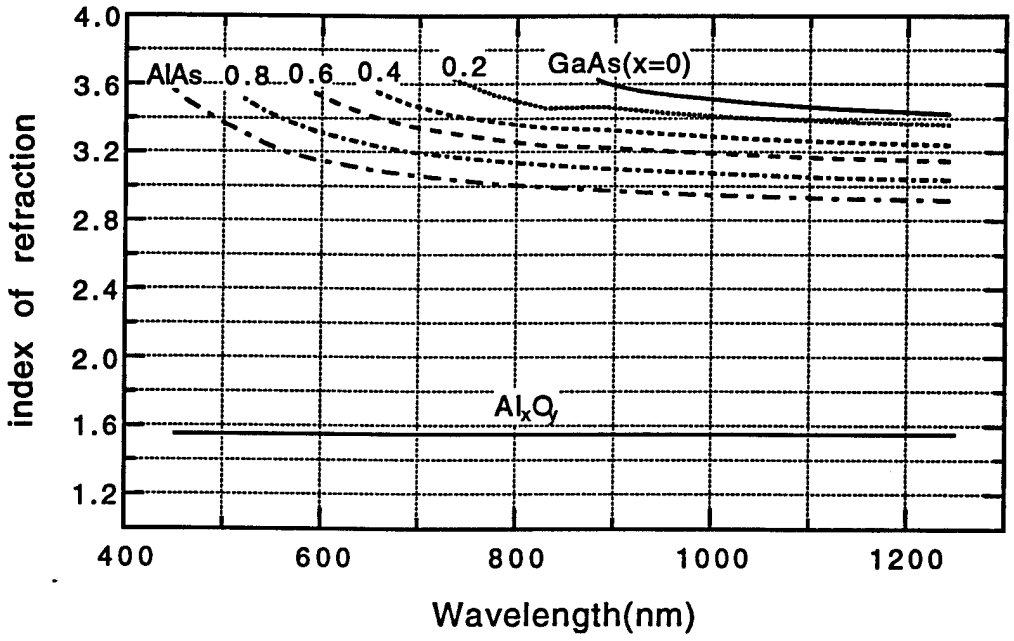

Figure 4.1: Refractive index vs. wavelength for various x-values of $Al_xGa_{1-x}As$.

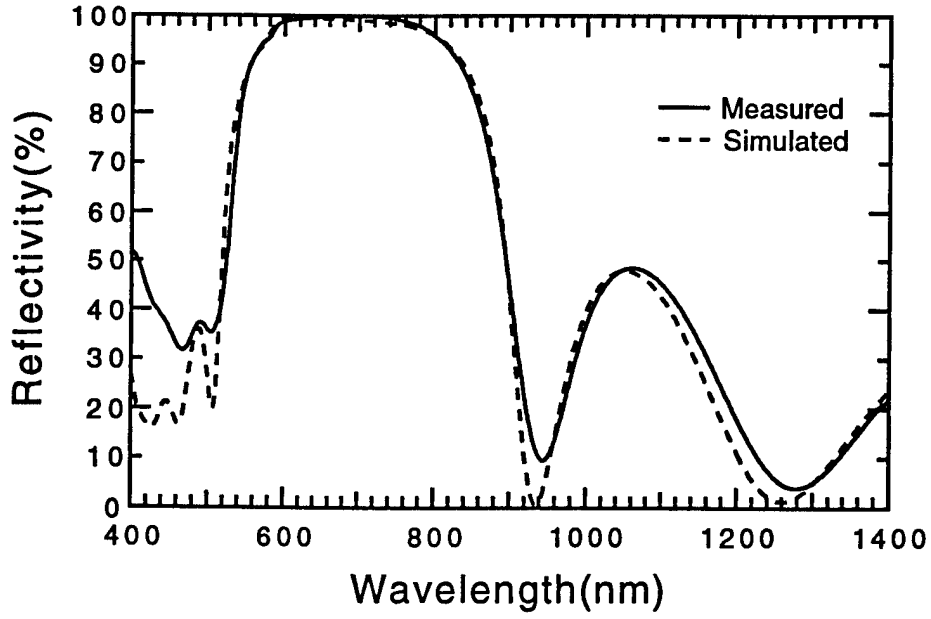

Figure 4.2: Measured and simulated spectrum of 4.5 period $Al_{.6}Ga_{.4}As/Al_xO_y$ DBR.

A number of possible mirror combinations have been investigated by OCI engineer Michael MacDougal in conjunction with other collaborators at the University of Southern California [6]. Both of these mirror combinations make use of the fact that AlAs or $Al_XGa_{1-X}As$ can be laterally oxidized to create low-index Al_XO_Y layers for the low index material in the DBR. We have already discussed lateral oxidation for current confinement in Section III. In Fig. 3.1, a pair of layers is oxidized in to confine current and optical energy. The oxidation time could be continued to completely oxidize the layer, resulting in a layer with refractive index between 1.5 and 1.56, depending on the oxidation conditions. Creation of this low index layer is the key element in the two alternative mirror technologies we discuss below.

The first combination of interest is Al_XO_Y in conjunction with $Al_XGa_{1-X}As$, where the x-value can now be 0.8, for example. The resulting refractive index ratio is (3.25-1.6)/(3.25+1.6)=0.34, compared to approximately 0.04 available with conventional $AlAs/Al_XGa_{1-X}As$ mirrors. The disadvantage of oxidized mirrors is that they are electrically insulating. This necessitates the use of an intracavity contact, but this has been demonstrated using Al_XO_Y/GaAs mirrors at 980 nm. The great advantage, of course is that mirror reflectivity is greatly enhanced with very few periods. If we use Al_XO_Y in conjunction with $Al_{.8}Ga_{.2}As$, with 5 mirror periods we are well over 99 percent reflectivity. Figure 4.2 illustrates the measured and simulated reflectivity spectrum for an $Al_XO_Y/Al_{.6}Ga_{.4}As$ mirror using 4.5 periods. The bandwidth is nearly 200 nm, which means the growth thickness tolerance is relatively loose.

Another promising mirror combination is the $Al_{.5}In_{.5}P/Al_XO_Y$ mirror, which is also lattice-matched to GaAs. This has even higher refractive index contrast and wider bandwidth than the $Al_XO_Y/Al_{.8}Ga_{.2}As$ mirrors, and the AlInP has a shorter wavelength band-edge than $Al_{.8}Ga_{.2}As$. Figure 4.3 illustrates measured and simulated spectra for this mirror pair. As illustrated, the short band-edge of the AlInP makes this mirror suitable for wavelengths down to 500 nm, if a suitable active region could be grown. A dramatic comparison with the conventional $AlAs/Al_{.5}Ga_{.5}As$ mirror is provided by Fig. 4.4. The bandwidth of the oxide-based DBR is 7 times larger than the conventional DBR, making the growth thickness tolerance 7 times looser.

Thus far, we have compared theoretical and experimental reflectivity *spectra*, with no measurement made of maximum absolute reflectivity. Measurement of absolute reflectivity is rather difficult, and it is simpler to incorporate the oxide-based DBRs into VCSEL cavities to examine if any excess scattering loss is present. This experiment has been performed by MacDougall et al for 980 nm VCSELs employing $GaAs/Al_XO_Y$ DBRs

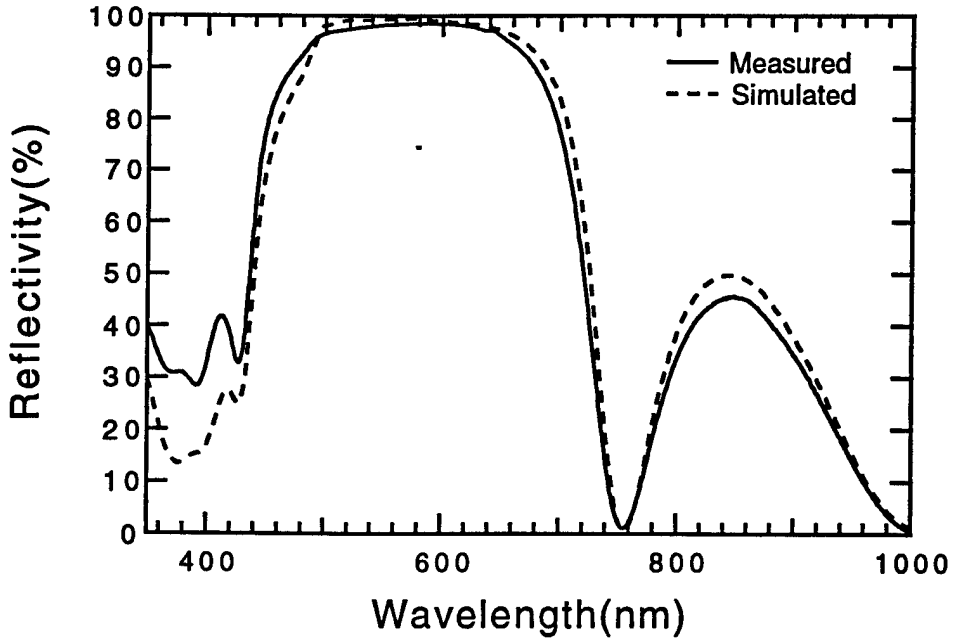

Figure 4.3: Measured and simulated spectra for AlInP/Al_xO_y mirror. Note usable bandwidth to 500 nm.

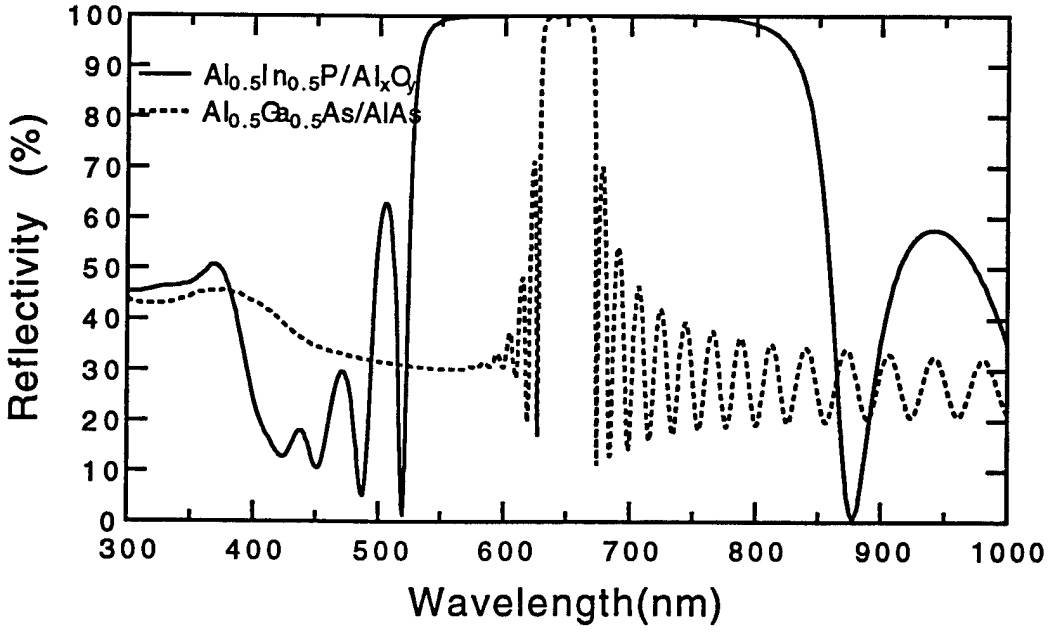

Figure 4.4: Comparison of oxide-based and semiconductor-based DBR. The wide bandwidth of the oxide-based mirror greatly relaxes growth tolerances.

[7]. The results indicate very low internal losses, which verifies that the oxide-based DBR absolute reflectivities are close to theoretical values.

V. Transparent Substrate 780 nm resonant cavity LED's.

Our original intention was to fabricate bottom emission red VCSELs-fused to GaP, but as described earlier, a red VCSEL wafer was not available during phase I of this program. As a result. we performed our experiment using a 780 nm VCSEL wafer, using the epitaxial structure shown in Fig. 5.1. This epitaxy was grown by our subcontractor Sandia National Laboratories. We did not obtain lasing with this structure, primarily because of a marginal design. The theoretical output mirror reflectivity in the structure of Fig. 5.1 is 99%. Although theoretical gain calculations indicate that the 5 quantum-well active region is capable of supplying the required gain [5], these calculations do not account for heating, non-uniform pumping, or excess non-radiative recombination, and these additional effects likely prevented the structure from lasing.

As a result, we obtained wafer-fused 780 nm light-emitting diodes (LED's) instead of VCSELs. These devices still provide some indication that a properly designed 780 or 650 nm wafer-fused bottom-emission VCSEL structure could be fabricated. Figure 5.2 shows the device structure we obtain after wafer fusion, substrate removal, and processing. This structure allows us to pump the LEDs in 2 different ways. First, using, the contact to the n-mirror we turn the device on without ever pumping across the fused GaAs/GaP junction. Second, using the back contact, we pump across the fused junction. Comparing results of the two pumping schemes tells us something about the electrical quality of the fused junction.

Figure 5.3 shows the L-I and I-V charcteristics of some bottom emission devices, pumped both ways. The current constriction in these devices was accomplished by lateral oxidation, as described in Section III. Figure 5.2 shows that the L-I curves are virtually identical for the two pumping schemes, and from the I-V curves we see a small amount of additional voltage due to the fused junction. We have shown therefore that the fused junction forms an electrically conductive interface. The small additional voltage across the fused junction does not reduce the radiative efficiency of the LEDs, as exhibited by the two identical L-I curves. Of course, as we stated already in Section II, we could always avoid pumping across the fused junction and place the contact in the n-mirror in real devices. Figure 5.3, however indicates that a back contact is possible, for cases in which packaging considerations dictate a back contact.

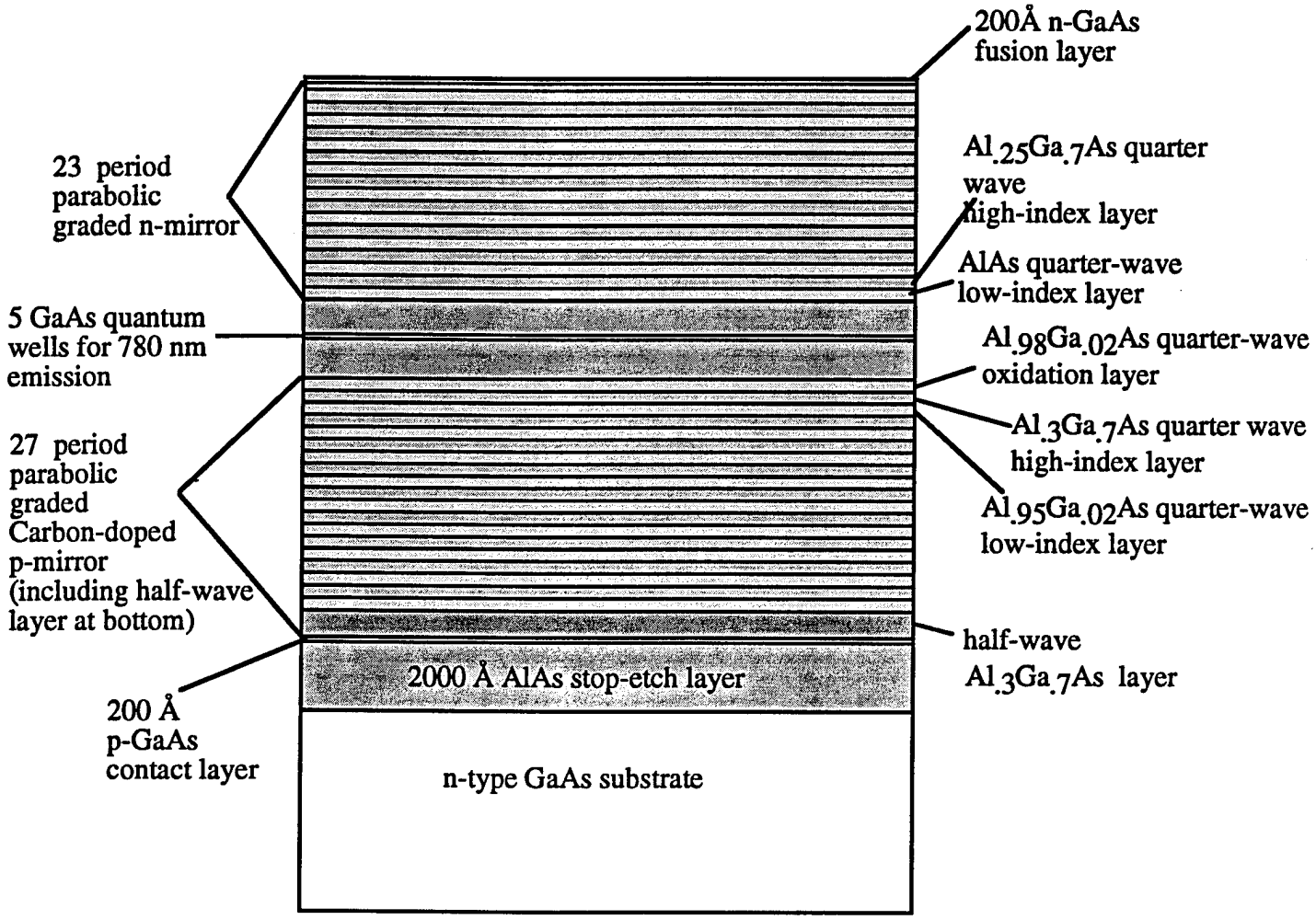

Figure 5.1: Initial epitaxial growth for 780 nm VCSEL wafer-fused to GaP. The structure is grown n-side up, so it will be p-up when it is fused to GaP and the n-GaAs\ substrate is removed.

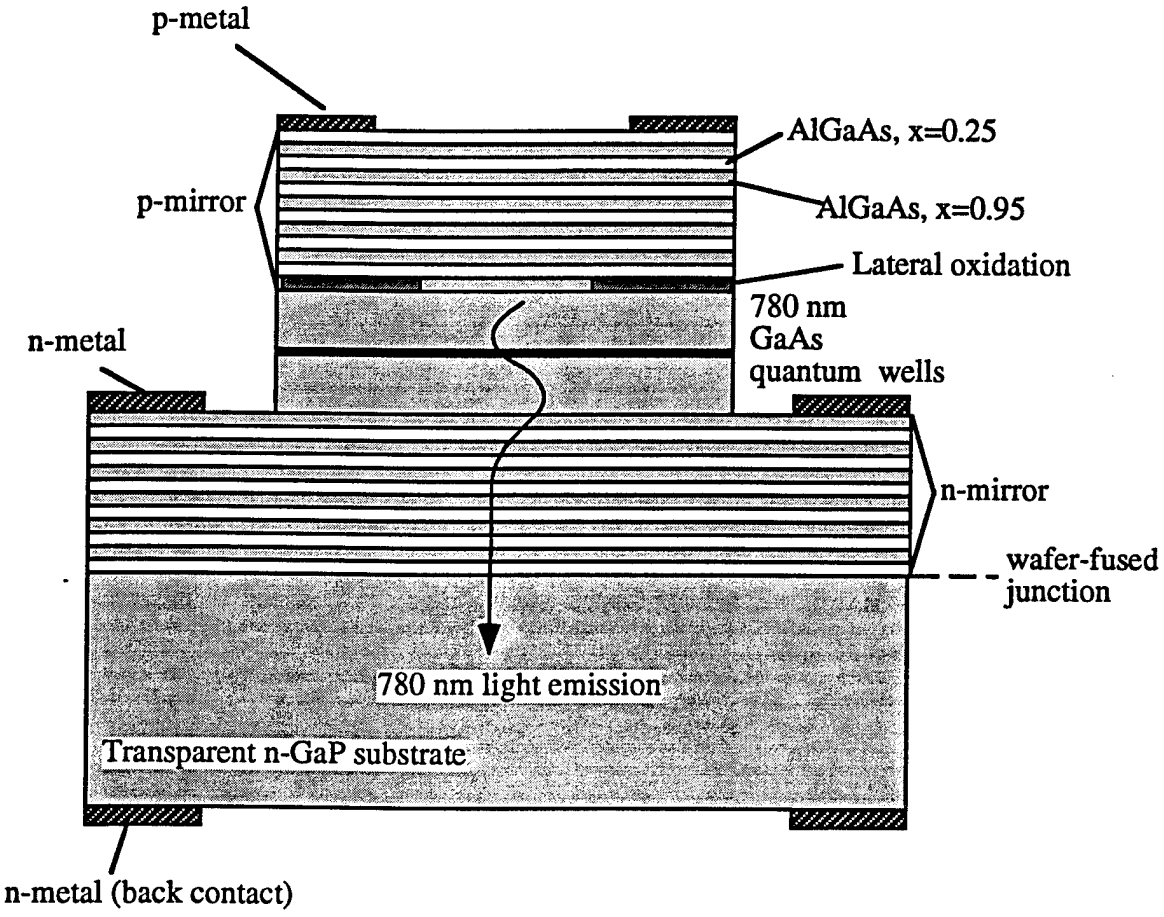

Figure 5.2: Bottom-emission 780 nm resonant-cavity LED. The structure has two n metal contacts, to allow comparison of pumping across the fused GaP/GaAs junction and pumping without crossing the junction.

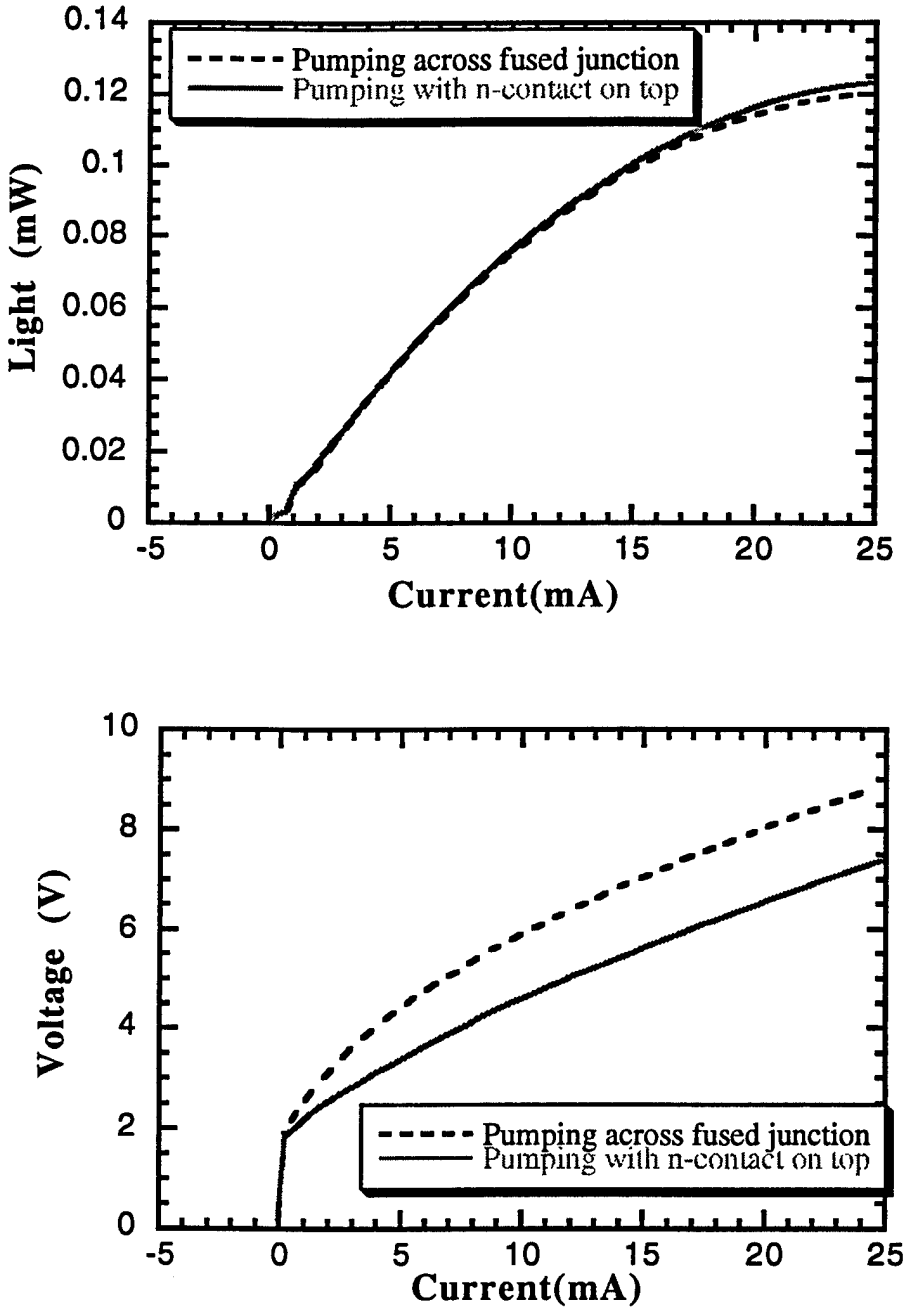

Figure 5.3: L-I-V curves for bottom-emission resonant-cavity 780 nm LEDs. The curves are shown for pumping with a back contact, which requires current injection across the fused GaAs/GaP junction, and for pumping with a contact in the n-mirror.

In section II, we showed in Fig. 2.4 an SEM picture of the wafer-fused 780 nm structure on GaP phosphide. This picture indicated no visible voids, which indicates negligible optical scattering loss due to the fused junction. Another indication of low optical scattering loss is the consistency of L-I curves and I-V curves like those in Fig. 5.3 from device to device. If air gaps were present, we would expect them to be randomly distributed, and to introduce a scatter in L-I and I-V curves. We do not observe these, so conclude that the GaAs/GaP interface is electrically and optically clean.

VI. Conclusion

We review here the objectives and accomplishments of this program.

1. Demonstrate wafer fusion of GaP to GaAs.

We have demonstrated good mechanical adhesion of GaAs to GaP, using a fusion time of 0.5 hour at 700 °C. After removing the GaAs substrate, no voids were visible in SEM photos of the fused interface. We found that an InGaP layer at the fused interface was unnecessary.

We subjected in-plane lasers to the wafer fusion thermal cycling, and compared devices before and after cycling. Both devices lased, but the device processed after thermal cycling exhibited approximately 30% increase in threshold current density and decrease in external efficiency. This may be the product of process variations, so we cannot say conclusively that the fusion thermal cycling degrades active regions. We used 1 hour at 700 °C, before later discovering that 30 minutes is sufficient. It is possible that 30 minutes fusion time leaves the AlInGaP/InGaP active regions undegraded.

We presented the possibility of low-temperature Palladium bonding as a possible replacement for wafer fusion, if it is later conclusively demonstrated that high-temperature wafer-fusion degrades InGaP quantum-well active regions. An aperture in the Palladium allows light passage out of the device. By using very thin 50 Å layers of Palladium, the resulting 50 Å air gap will not significantly compromise thermal impedance of the device.

We demonstrated good current conduction through the fused interface in wafer fused 780 nm bottom-emission resonant-cavity LED's.

2. Demonstrate Al_xO_y current-blocking layers in conventional (absorbing substrate) AlInGaP-based red VCSELs.

Our subcontractor Sandia National Laboratories has demonstrated room-temperature CW operation of red VCSELs at 645 nm and 652 nm using oxidation for current and optical confinement.

3. Demonstrate high-reflectivity AlInP/Al_xO_y distributed Bragg reflectors.

OCI engineer M. MacDougall, working at USC, has demonstrated both AlInP/Al_xO_y mirrors and $Al_xGa_{1-x}As/Al_xO_y$ wideband visible mirrors, which match theoretically predicted spectra. The latter mirror pair is compatible with established GaAs/AlGaAs growth technology. Both mirror combinations loosen tolerances on growth thickness. The high absolute reflectivity of oxide-based mirrors has been verified in 980 nm VCSELs using GaAs/Al_xO_y mirrors.

4. Demonstrate transparent-substrate VCSELs using wafer-fusion to GaP substrates and selective oxidation for current injection.

Because a red VCSEL wafer was unavailable, we attempted to perform this experiment using a 780 nm VCSEL wafer, which would also emits light that would be absorbed in a conventional GaAs substrate. We completed fabrication, but the devices did not lase. We were able to show however, bottom-emission resonant-cavity LED operation, and good I-V characteristics through the fused junction. We also showed little difference in LED performance when comparing a backside n-contact (pumping through fused junction) with a top-side n-contact (not pumping through fused junction).

5. Fabricate transparent-substrate visible VCSELs using wafer fusion (objective 1), selectively oxidized current blocking layers (objective 2), and AlInP/Al_xO_y distributed Bragg reflectors (objective 3).

Had the VCSELs in objective 4 lased, we would have completed objective 5 without the AlInP/Al_xO_y mirrors, but because we did not obtain lasing in objective 4, objective 5 remained uncompleted. We showed however that AlGaAs/ Al_xO_y is perhaps a better near term choice for a short-wavelength mirror, since it relies on more established growth technology.

In summary, we have concluded during this program that red VCSELs can operate at plastic fiber communication wavelengths, and can be fabricated as bottom-emission devices with flip-chipping. It remains unclear if wafer fusion can be accomplished with absolutely no degradation of InGaP active regions, but Palladium bonding can also be used to make bottom-emission devices. Lastly, the $Al_XGa_{1-X}As/Al_XO_Y$ mirror combination is a promising candidate for improved performance at 650 nm, as well as wavelength reduction to the Helium-Neon 632 nm wavelength.

References

1.. Schneider, R.P.,Choquette K.D.; Lott, J.A.; Lear K.L.; and others,"Efficient room-temperature, continuous-wave AlGaInP/AlGaAs visible (670 nm) vertical-cavity surface-emitting laser diodes," *IEEE Photonics Technology Letters*, 1994 MAR, V6 N3:313-316.

2. Lear, K., Choquette, K.D. , Schneider, R.P., Kilcoyne, S.P., and Geib, K.M., "Selectively oxidized vertical-cavity surface-emitting lasers with 50% power conversion efficiency," *Electron. Lett.*, 1995, **31**, (3), pp. 208-209.

3. Dudley, J.J. "Wafer-fused Vertical Cavity Lasers," Ph.D. Dissertation, University of California at Santa Barbara, August, 1994.

4. Jayaraman, V. "Wavelength-division-multiplexed high-speed distributed fiber-optic data communication system Using InGaAsP/InP-based 1.3/1.55 micron vertical-cavity surface-emitting lasers," quarterly report number 5, BMDO SBIR contract number DASG60-94-0022.

5. Choquette, K.D., Schneider, R.P., Crawford, M.H., Geib, K.M., and Figiel, J.J., "Continuous-wave operation of 640-660 nm selectively oxidized AlInGaP vertical-cavity lasers," *Electroni cs Letters,* July 6, 1995, vol. 31, no. 14, pp. 1145-1146.\

6. Corzine, S.W. "Design of Vertical-Cavity Surface-Emitting Lasers with Strained and Unstrained Active Regions," Ph.D. Dissertation, University of California at Santa Barbara, May 1993.

7. MacDougal, M.H., Ph.D. Dissertation, Chapter 4, University of Southern California, to be published 1996.

8. MacDougal, M.H., Yang, G.M., Bond, A.E., Lin, C.K., Tishinin, D., and Dapkus, P.D., "Electrically pumped Vertical-Cavity Surface-Emitting Lasers with AlxOy-GaAs reflectors," *Photonics Technology Letters,* vol. 8, no. 3, pp 310-312.